Understanding phase transition in the ZnSiP2 chalcopyrite, a quantum chemical topology study

Khadra Tahri, Tarik Ouahrani, Julien Pilmé

Noname manuscript No.
(will be inserted by the editor)

Understanding phase transition in the $ZnSiP_2$ chalcopyrite, a quantum chemical topology study

Khadra Tahri [1] · **Tarik Ouahrani**[1,2] · **Julien Pilmé**[3,4]

Received: date / Accepted: date

Abstract Understanding the behavior of the matter under pressure is crucial for the development of novel polymorph of the chalcopyrite compound. Herein, we study the evolution of the bonding of $ZnSiP_2$ up to 100GPa. We particularize our results by means of the detailed *ab initio* study of its structural and dynamical properties. In fact, the compound show disordered structure at 32GPa which transform at 82GPa to an denser ordered one with 8 fold coordination. We show how the electron localization function can be useful to modulate the effect of compression along the proposed transition path. The integration of basin attractor reveals that the breaking of Si–P bonds are the key of formation of denser SiP_8 units at high pressure.

Keywords *ab initio* calculation · basin attractor · pathway transition

1 Introduction

Subjecting the ternary chalcogenides compounds to extreme conditions likes high-pressure can reveal more interesting properties [1], because of the structure transformation and the improved electronic properties, which can directly influence their photo-voltaic applications [2]. For instance, using energy dispersive X-ray diffraction, Gonzalez and Rincon [1] investigated the optical absorption edge of the monocrystalline structure $CuInS_2$ under pressures up to 10 GPa, they found that $CuInS_2$ undergoes a phase transition from tetragonal structure with tetrahedral coordination

K. Tahri
[1]Laboratoire de Physique Théorique, Université de Tlemcen, 13000 Tlemcen Algeria.

T. Ouahrani
[1]Laboratoire de Physique Théorique, Université de Tlemcen, 13000 Tlemcen Algeria.
[2]École supérieure des sciences appliquées, B.P. 165, 13000 Tlemcen, Algeria.
E-mail: tarik_ouahrani@yahoo

J. Pilmé
[3]Laboratoire de Chimie Théorique, UMR 7616 CNRS, UPMC Univ. Paris 06, Sorbonne Universités, Case Courier 137, 4 place Jussieu, 75252 Paris Cedex05, France
[4]CNRS UMR 7616, 4 Place Jussieu, 75252 Paris Cedex 5, France
E-mail: pilme@lct.jussieu.fr

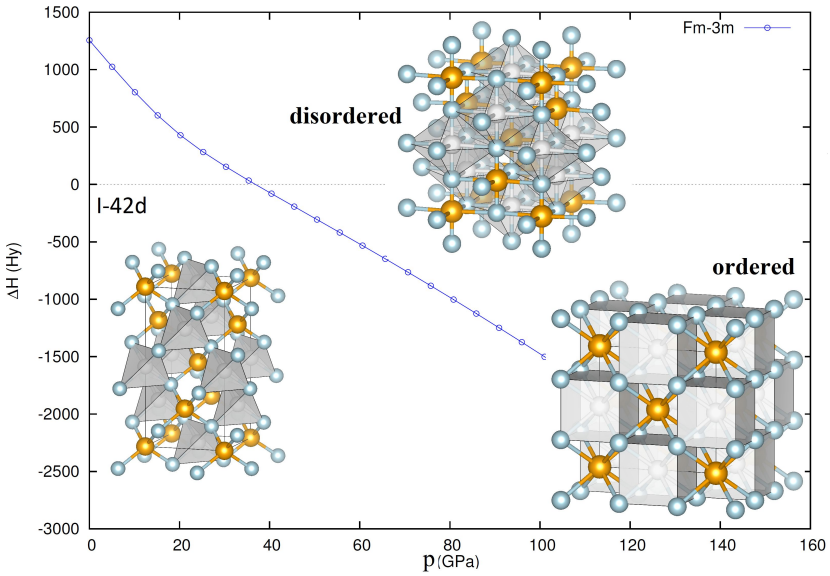

Fig. 1 Enthalpy difference for all phase transitions involving $ZnSiP_2$ polymorphs vs. pressure. Crystallographic structures of the three phases are represented in the inset.

to cubic structure with octahedral coordination. This phase transition dramatically changes the optical and electrical properties of the compound due to the decrease in inter-atomic spacing of the InS_4 polyhedron. In fact, when the transformations are induced by pressure, the outstanding capability of this variable is to promote high metal coordinations in crystalline solids.

Basically, the rationalization of the changes in symmetry pattern along a phase transformation in a solid is done by performing dynamical simulation trajectories [3,4]. However, the existence of one or more group-subgroup pathways linking the two end phases, allows us to imply a collective movement of atoms along the way of phase transitions. In this approaches, atomic displacements and its mechanism became accessible to first-principles calculations [5].

Due to its nonlinear optical properties [6] or as solar cell material [7], zero pressure phase has been one of the most widely studied phases in the $ZnSiP_2$ compound. For the effect of pressure, Arab et al. [8] done a preliminary *ab initio* investigation on the title compound, where they study its phase transition to NaCl phase. In this work, the authors give some trend of electronic and elastic properties under pressure. Very recently, in order to establish a possible new II-IV-V_2 polytypes, Bhadram et *al.* [9], performed an experimental studies of the $ZnSiP_2$ up to 35GPa. In this work, X-ray diffraction (XRD) and Raman scattering mesure inside a diamond anvil cell (DAC) shown an order-disorder phase transition mechanism for this material between 27 and 30GPa. In our early work [10], we took a special point of view to investigate chemical relevant magnitudes that affects the $ZnSiP_2$ chalcopyrite under pressure. The analysis of charge density within Quantum Theory of Atoms in Molecules (QTAIM) approach [11] demonstrate unequivocally that partitioning the observables of physical systems into additive microscopic contributions [12,13] shed light on the local properties under pressure[14]. In this work[10], we have determined

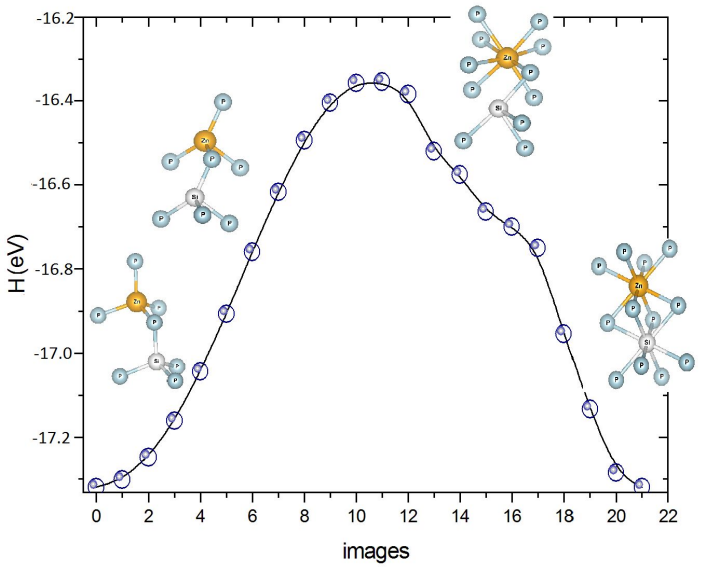

Fig. 2 Calculated enthalpy profile along the (Cc) path transition

local compressibilities for both semi-conducting and metallic phase of the title compound. However, we fail to delight an appropriate mechanism able to depicting the microscopic image of the phase transition in this compound.

Moreover, our contribution aimed at a full understanding of the interplay between unit cell structural changes, energetic profiles, and chemical bonding reorganization of $ZnSiP_2$ under effect of pressure. To go further in the behavior of the $ZnSiP_2$; we intend to analyze its response to a pressure up of 100 GPa. Our efforts are to put forward the understanding of how the chemical bonding network changes from zero to higher pressure. Among many quantum chemical topological formalism, the electron localization function (ELF)[15,16] is one of the most appropriate numerical tools to offer a clear view of those regions within the unit cell that are especially sensitive to chemical activity under pressure.

The present paper is organized in three sections. In the next one (see section 2), we present the computational tools used in this study. In a first product of our investigation (see section 3), we provide theoretical data on the structural and equation of state (EOS) parameters of the title compound as well as in its low and high pressure phases; compared with the sparing available experimental and theoretical results. The second finding deals with the pictures that ELF provides to understand how pressure affects bonding properties of the $ZnSiP_2$ compound. The reasoning behind this choice is that we can uniquely identify regions of crystal whose are more affected by pressure. By means of ELF, we will discuss also the formation of new bonds at the path transition. A brief summary and the main conclusions are gathered in Section 4.

2 Computational details

Ab initio simulations were performed within the framework of density functional theory (DFT) and the pseudopotential method as implemented in the Vienna *ab initio* simulation package (VASP). We used the projector augmented wave (PAW) all-electron description of the electron-ion-core interaction [17]. The GGA [18] level has been used for exchange correlations. The Monkhorst-Pack scheme was employed for the Brillouin zone integration in each structure. We used a dense mesh of **k** points to obtain a high precision in the calculation of energies (about 1 meV per formula unit) and the forces on the atoms. At each selected volume, the structures considered here were fully relaxed to their equilibrium configuration through the calculation of the forces and the stress tensor until the forces on the atoms were smaller than 0.004 eV/Å and the deviation of the stress tensor from a diagonal hydrostatic form was less than 1 kbar. To simulate the disorder in the NaCl phase we used a of 2×2×2 super cell by forcing VASP to no considering any symmetry.

The Electron Localization Function (ELF) was originally designed by Becke and Edgecombe to identify localized electronic groups in atomic and molecular systems[15] in a Hartree-Fock framework. From this seminal definition, several interpretations were given, for example, in the context of Markovian processes [19,20]. However, the most intuitive interpretation is that proposed by Savin et al [21] in the DFT framework for which ELF can be understood as a local measure of the excess of local kinetic energy of electrons, $t_p(\mathbf{r})$, due to the Pauli principle. This quantity is computed by subtracting the bosonic contribution, $|\nabla\rho(\mathbf{r})|^2/8$, from the kinetic energy density of the system, $t(\mathbf{r})$. Re-scaling it with respect to the homogeneous electrons gas like in the original definition provides the core of ELF, $\chi(\mathbf{r})$:

$$\chi(\mathbf{r}) = \frac{t_p(\mathbf{r})}{t_w(\mathbf{r})} = \frac{t(\mathbf{r}) - \frac{1}{8}\frac{|\nabla\rho(\mathbf{r})|^2}{\rho}}{c_F\rho^{5/3}(\mathbf{r})} \tag{1}$$

where c_F is the Fermi constant. According to this definition, the regions of electron pairing would have a small χ value. In order to inverse this relationship and map it in a closed interval, the final function was defined as follows:

$$\eta(\mathbf{r}) = \frac{1}{1+\chi^2(\mathbf{r})} \tag{2}$$

It can be easily seen that ELF runs from 0 to 1, and equals to 0.5 in the uniform electron gas. Note that this expression has also been defined an a quasirelativistic context. [22] In contrast to the topology of the electron density (QTAIM methodology), the ELF topology provides a non-atomic partition into localized electron pairs regions (basins). Each basin is presented with a chemical meaning : core basins, labeled K(A), in core regions of A atoms; outer–core, labeled L(A) or M(A) ; lone-pair basins, labeled LP(A), and bonding basins, labeled B(A–B) located along the A–B bond axis. The basin populations (noted $\bar{N}$) are determined by integration of the electron density over the basin volumes. These quantities are used for rationalize the bonding schemes in molecules or in solids.

All electron wave functions are preferable for a quantitative analysis of the ELF topology in a crystalline phase. Thus, ELF and electron density maps along the bond path were obtained using DGRID [23] interfaced with ELK [24], a code implementing the all-electron full-potential linearized augmented-plane wave (FPLAPW)

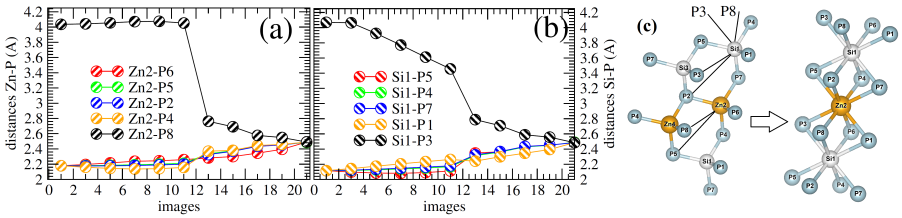

Fig. 3 Evolution of the (a) Zn–P and (b) Si–P bonds along the intermediate images of the Cc path. (c) is a polyhedral representation of the relevant changes in the bonds.

method. The partition into basins and the integration of the electron density were also performed with DGRID.

To perform analysis on non-covalent bonding, we use the Non-Covalent Interaction (NCI) [25] index as a new topological tool based on reduced density gradient RDG (s). In fact, the origin of the RDG can be traced to the GGA exchange energy contribution, E^X_{GGA}, from DFT theory:

$$E^X_{GGA} - E^X_{LDA} = -\boldsymbol{\Sigma} \int F(s)\rho^{4/3}(\boldsymbol{r})d\boldsymbol{r} \tag{3}$$

where $F(s)$ is a function of s for a given spin with

$$NCI = s = \frac{1}{2(3\pi^2)^{1/3}} \frac{|\nabla\rho|}{\rho^{4/3}} \tag{4}$$

The 4/3 exponent of the density ensuring that s is a dimensionless quantity. s accounts for local density in homogeneities due to its differential behavior depending on the chemical region of the crystal. The key of NCI isosurface is based on the sign of the second eigenvalue of the Hessian (λ_2) times the electron density ρ. If the sign is negative, the attractions are judged attractive and colored in bleu. However, if it is a positive, the attractions are rather repulsive in red. In the case of $(\lambda_2) * \rho$ is close to zero, weak interaction like van der Walls interactions including dispersion situation are invoked.

3 Main calculated results

3.1 Structures and stabilities

To elaborate our martensitic procedure, we have began by performing an atomistic *ab initio* calculation within a range of pressure up to 100GPa under the static approximation (zero-temperature and zero-point vibrational contributions neglected). Two structures were investigated, I-42d, and a 2×2×2 super cell of Fm-3m ones. In fact in the first stage of our calculation we put the phosphorus atom at (0.5,0.5,0.5) and the Zn/Si ones at (0,0,0) position with a degree of stoichiometry of 50% [9]. The NaCl structure changes a lot with increasing pressure. The Bilbao Crystallographic Server symmetry utilities [26] allows us to distinct two structures, the first at low

Table 1 Calculated optimized parameters, bulk modulus and elastic stiffness of the three phases of the $ZnSiP_2$, I-42d at 0.00GPa, and Fm-3m$_2$ at 82.00GPa. All C_{ij} are done with (GPa).

a (Å)	c(Å)	B_0	C_{11}	C_{12}	C_{13}	C_{33}	C_{44}	C_{66}
I-42d								
5.42^a	10.53^a	85.35^a	135.71^a	57.10^a	63.26^a	129.52^a	69.34^a	66.20^a
5.40^b	10.50^b	86.29^b	136.68^b	54.79^b	60.79^b	133.11^b	71.91^b	69.63^b
5.39^c	10.44^c	–	–	–	–	–	–	–
Fm-3m$_1$								
4.75^a	–	176.65^a	–	–	–	–	–	–
Fm-3m$_2$								
5.45^a	–	378.48^a	409.43^a	363.00^a	–	–	202.11	–

^{a} this work, ^{b}from ref [8] ^{c}X-ray data ref. [27]

pressure is distorted and the second at high one is rather ordered. We will call it : Fm-3m$_1$ and Fm-3m$_2$. The juxtaposition with the available structural properties of I-42d phase leads us to say that our theoretical calculations are comparable to the results from ref. [8], and with a reasonable discrepancies with regard to X-ray data from refs. [27] (see table 1). However, for the structure found low pressure, it is very difficult to make any comparison with the experiment. The sole experimental investigation, for the moment, made by Bhadram et al. [9], does not present any indication on the shape and atomic positions of the structure of the compound at the transition pressure. All what we learn from this cited work is that $ZnSiP_2$ undergoes, under pressure between 27 GPa and 30GPa, a phase transition from tetragonal structure with tetrahedral coordination to disordered structure with octahedral coordination (This disordered phase shows some orthorhombic distortion in its lattice parameters). To determine all possible transition pressure, we have evaluated how the difference between the enthalpies ΔH of all structures changes with pressure. The polymorphic sequence we found is I-42d $\longrightarrow$ Fm-3m$_1$ for a pressure equal to 32.22GPa respectively (see figure 1). However, towards the 82GPa, while maintaining the same space group with some difference in the coordination (Fm-3m$_2$), a transformation in polyhedral from 6 fold to 8 fold occurs.

To confirm the stability of the predicted structures at 0, 32.22 and 82GPa, we have calculated their elastic stiffness and mechanical stability. Calculated single-crystal elastic constants (C_{ij}) at their stable pressures for the investigated structures are listed in Table 1. It is noted that the C_{ij} values for zero pressure phase predicted within the same approach (with CASTEP Package [8]) as for the present work, are very close to the ours. For tetragonal system, the Born stability criteria [28] are: $C_{11} > |C_{12}|$, $(C_{11} + C_{12})C_{33} > 2C_{13}^2$, $C_{44} > 0$ and $C_{66} > 0$. In the other hand and for the Fm-3m$_2$ crystals at 82 GPa, the mechanical stability requires the elastic constants satisfying the well-known Born stability criteria [28] : $C_{11} > |C_{12}|$; $C_{11} + 2 \times C_{12} > 0$ and $C_{44} > 0$. Depending on the stability criteria, we can confirm the existence of an ordered structure with Fm-3m$_2$ space group. However, due to the distorted and disordered nature of the Fm-3m$_1$ structure, we could not be able to confirm its stability. In fact, the phase at 32.22 GPa requires a dynamical disordered calculation, which is, unfortunately, not allowed within the *ab initio* calculations at absolute zero temperature.

3.2 Phase transition mechanism

The second step we have followed is to find a common space subgroup of both the initial and final structures in the studied transition. The representation of the initial and final phases in the basis of the common subgroup allows a direct comparison with the possibility of visualizing all the changes in the lattice parameters and atomic coordinates associated with the transformation. As a reasonable transformation from (I-42d) to (Fm-3m_2)(no order-disorder mechanisms are considered in the utilities of ref.[26]). We have chosen a phase transition path based on the monoclinic subgroup Cc (#09) with 16 atoms (Z_H=4). The pathway 4 $\longrightarrow$ 8 involves atomic displacements of (Δ_{tot}=1.97810Å) with lattice strains ($\mathcal{S}_{tot}$=0.1862) [29]. The transformation matrices $(P,p)_1$ for (I-42d) to (Cc) and $(P,p)_2$ for (Fm-3m_2) to (Cc) are respectively {-**c**,**a**+**b**,1/2**a**-1/2**b**+1/2**c** } and {-1/2**a**-**b**-1/2**c**,1/2**a**-1/2**c**,2**a**+2**b**+2**c** }. The enthalpy energy profile of the 4 $\longrightarrow$ 8 mechanism is shown in figure 2 where H is represented versus the optimized images. The calculated transformation enthalpy barrier for the 4 $\longrightarrow$ 8 fold gives 91.661kJ/mol. The transition states (TS) for the this transformations is found at image number 11 (see figure 2).

To track the chemical bonding changes in the 4 $\longrightarrow$ 8 fold, we have firstly measured the distances progress along the Cc path. On figures 3(a–b), we give the variation of the Zn–P and Si–P bonds as a function of images change pondered with the representation of the two end phases of the intermediate structure. In the inset of figure 3(c), the Zn atom (labeled as Zn2) is surrounded by four P atoms (labeled as P6, P2, P4 and P7) while the Si one (labeled as Si1) is surrounded by four P atoms (labeled as P5, P1, P4 and P7). Here, the c/a ratio sees its value increasing from 0.85 to 1.42 along the 22 transformations images. Thus, we will discuss our results according to the images evolution. The ZnP_4 and SiP_4 tetrahedral units show four different distances: Zn2-P5= Zn2-P4, Zn2-P6, Zn2-P2 and Zn2-P8=Zn2-P5=Zn2-P3=Zn2-P1, where the first three units have shown a smaller dilatation by a 0.32 Å, while the Zn2-P8 bond reduces drastically by 1.55 Å. In fact, where the ZnP_8 is formed at the TS structure (image number 11): Zn2-P8 undergoes a brute change. The P6-Zn2-P2 angle is also affected and is opened by around 67.778°, whereas the P6-Zn2-P7 one is closed by 38.437°. The analysis of figures 3(b) and (c) confirm that the evolution of Si-P bonds along the Cc path is comparable to the Zn-P ones; the only difference is that the SiP_8 is formed at final stage and not at TS structure. The change in distances and angles across the 4–8 fold transformation is a consequence of the simultaneous changes in both lattice parameters and atomic positions.

3.3 Bonding analysis

3.3.1 Electron localization function analysis

Due to the topological partition induced by ELF, the 3D space of the I-42d and Fm-3m_2 unit cells can be distributed in localization basins associated to meaningful chemical entities (see figures 4(a) and 4(b)). Locations of ELF maxima (attractors) and the ELF population analysis for $ZnSiP_2$ in the zero and that of 82 GPa structures are shown in Table 2, figures 4(c) and 4(d). The first outstanding feature of the ELF analysis is that the electron pairs are distributed in both structures, forming closed atomic electronic shells around the nuclei: three core K-shell, K(Zn), K(Si) and

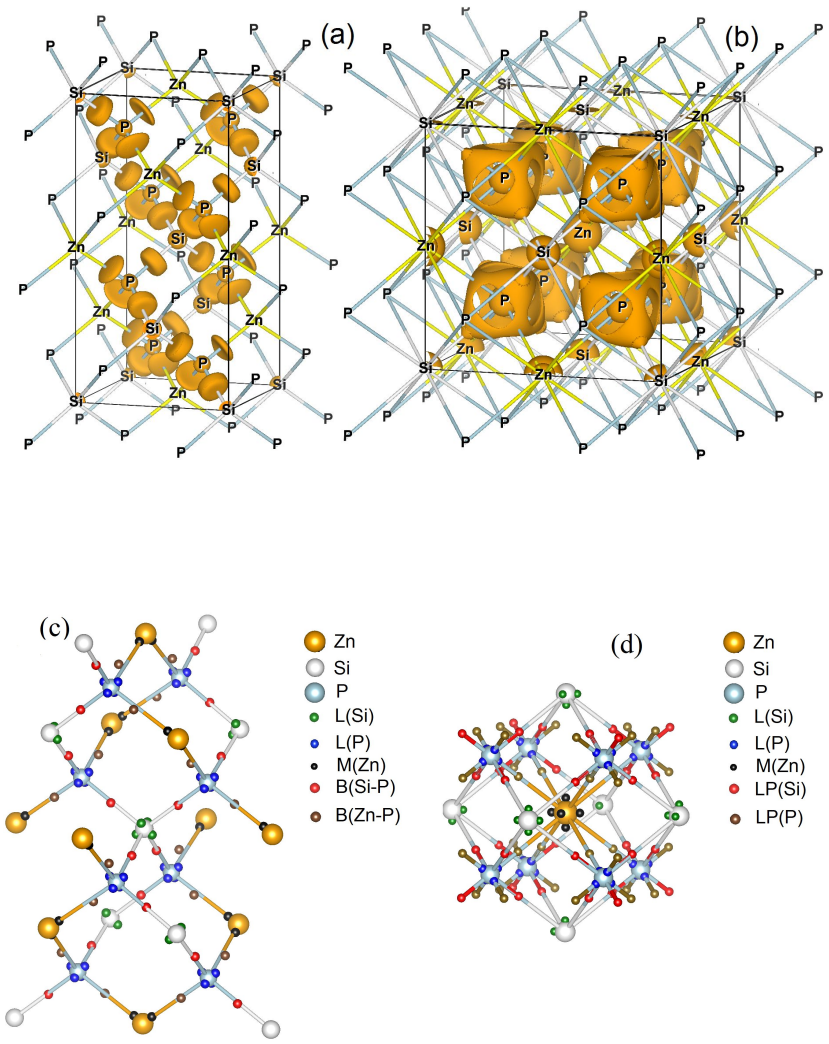

Fig. 4 Top ELF localization domains for $ZnSiP_2$, (a) isosurface = 0.86 for I-42d and (b) isosurface = 0.76 for Fm-3m$_2$. Down, 3D locations of ELF attractors (maxima) for (c) I-42d and (d) Fm-3m$_2$ structures.

K(P), an outer-core L-shell for the silicon and phosphorus atoms, and an outer-core M-shell for the Zinc one, and finally some bonding basins B(Si–P) and B(Zn–P) located along the axis of bonds. Due to the symmetry of the cell and the atomic positions, multiplicity of equivalent atoms has to be taken into account when Table 2 is analyzed. The set of basins surrounding the phosphorus cores in both I-42d and

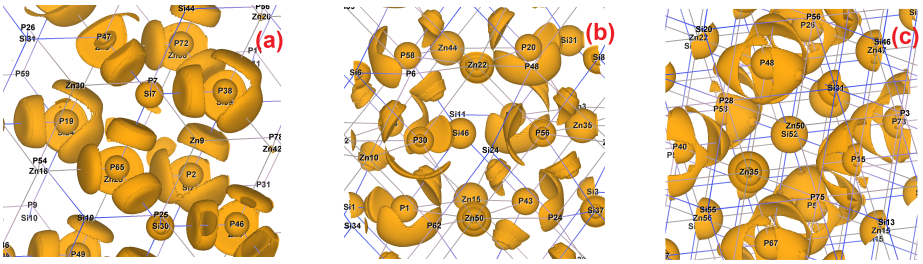

Fig. 5 ELF localization isosurface along three image in the Cc transition path, (a) image 1, (b)image 11 and (c) image 22, $\eta = 0.84$.

Fm-3m$_2$ structures. The locations of ELF maxima indicate that the Si–P bond is rather covalent while the Zn–P is rather ionic since B(Zn–P) basins are very closely packed with P atoms. This result is consistent with the difference of electronegativity between Zn and Si atoms. The analysis of the Fm-3m$_2$ structure reveals that the ELF maxima for in both bonds decreased with a closer magnitude. In the Fm-3m$_2$ structure, the nature of bonds Zn-P and Si-P remain unchanged. However, as shown in Table 2, the basin populations differ in these structures (I-42d and Fm-3m$_2$) which reflect the new coordination. We would like to bring the attention to the geometrical arrangement of the Si and Zn outer core attractors which are of number of 6, contrary to the P atom which has 8 L-shell (see figures 4(c) and 4(d) and the multiplicity in table 2). As previously reported in other studies [30,31], the position of these attractors minimizes their mutual repulsion because (outer)core electrons obey to the same rules as valence ones.

To understand all changes induced by hydro-static pressure in the compound $ZnSiP_2$, we have chosen to analyze the evolution of ELF basins across the transition path. Figure 5, clearly reveals that the most relevant chemical changes are suffered by the P valence. We observe that the B(Zn–P) basins is split firstly before that of B(Si–P) ones, see figure 5(b). The new attractors are initially located along the two planes that bisects the angles formed by the Si/Zn atoms and the four approaching P atoms. Here the valence is divided into four pairs of equivalent basins. In fact, if we observe image 11 corresponding to the transition state in the Cc path, we can clearly observe that each B(Si–P) basin splits,in the Fm-3m$_2$ structure, into two basins LP(Si) and LP(P) which are formed along the Si–P axis, one on the side of Si and the other on the side of P atoms (see figure5(b)). This indicates a typical covalent bond process between P and Si atoms [32]. The same thing happens to the two approaching atoms from the nearest neighbors. In addition, the basin populations of B(Si–P) basins seems to depend on the local chemical environment. Indeed, three populations show values varying between 1 and 2 electrons, respectively $\sim$2.69, $\sim$2 and $\sim$1.2 electrons whereas the last one has a smaller population lower than 1 electron. Note that value of ELF maxima for this latter is also smaller that the other ones (See Table 2).

In order to achieve an accurate description of the studied transformation, we can track the emerging bonds by use of 1D-ELF profile. On sub-figures 6, we plot the evolution of two distances from those measured in figure 3(c), in black line (left panel), the P8-Zn2-P6; and in orange line (right panel) the P2-Si1-P1 one. Here the Zn2-P6/Si1-P1 connect the equatorial bond and P8/P2 is the approaching phosphorus atom. This profile gives an important chemical information about the emerging

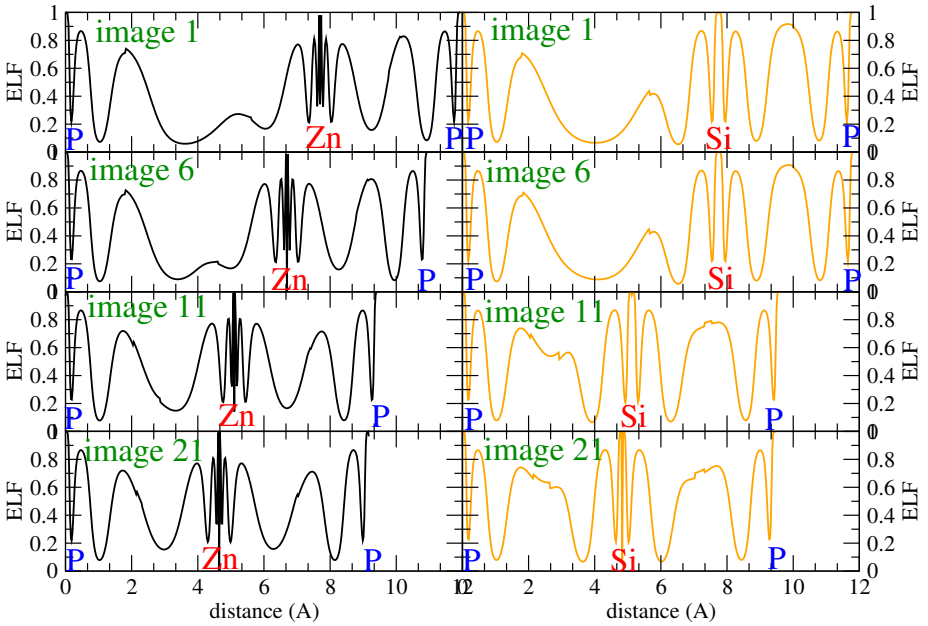

Fig. 6 ELF profiles at the transition pressure along a line with Si/Zn nearest and next nearest P neighbors for image 1(I-42d), image 6, image 11 (TS state) and image 21 (Fm-3m$_2$)

Table 2 volume (Bohr^3), populations (electron), ELF maxima η and multiplicity (M) of the ELF attractor for I-42d and Fm-3m$_2$ structures.

	volume	populations	η	M	attractor
I-42d					
	1.8	1.9	0.868	32	L(P)
	5.5	4.2	0.776	16	M(Zn)
	1.8	2.1	0.868	16	L(Si)
	68.3	2.0	0.887	16	B(Zn-P)
	52.6	2.0	0.927	16	B(Si-P)
Fm-3m$_2$					
	1.2	2.1	0.866	32	L(P)
	3.6	2.7	0.773	24	M(Zn)
	2.1	2.9	0.867	24	L(Si)
	9.3	0.6	0.702	32	B(Zn-P)
	25.9	1.5	0.762	32	LP(P)

bonds. While the ELF topology seems not affected along the transformation images, the profiles representing the Zn2-P8 and Si1-P2 bonds undergo a real revolution. We can see approaching bonds along their equatorial directions. The small relief (between 2.5–4.0 Å in image 1 of figure 6) is related to the shadow P5 atom of Zn2-P5/Si1-P5 bonds not discussed now. It is apparent that the Zn2-P5/Si1-P5 distances decrease and began equal to its connecting Zn2-P6/Si1-P1 ones, and at the same time, their ELF maxima change ($\eta = 0.705/0.758$). Because each curve has a 2-fold multiplicity, we can conclude that the ELF profile between the two minima around ∼1.5 and ∼3.5 Å is a clear signature of the Si–P/Zn–P chemical bond in $ZnSiP_2$.

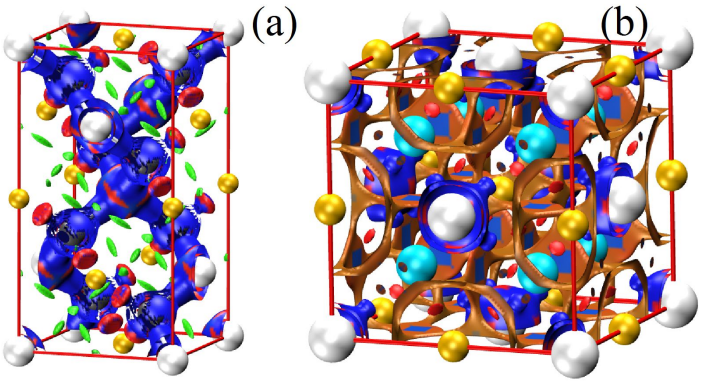

Fig. 7 3D NCI plot for (a) I-42d structure and (b) Fm-$3m_2$ one.

3.3.2 Noncovalent interaction analysis

Furthermore, we have analyzed our calculated charge density by using the NCI (noncovalent interaction) index [25] which is more adapted for identifying weak noncovalent bonds than the electron localization function (ELF). NCI regions enclose interstitial critical points, so they provide a faithful representation of the atomic bonding network, as defined by Atom inside molecule procedure. To provide an easy-to-visualize way for recognizing cation-anion and anion-anion contributions to the $s(\rho)$ plot, a three-dimensional NCI isosurface representation is preferable (see figure 7). We can find in the I-42d cell, localized strong attractive interactions isosurfaces which appear around the phosphorus atom, yielding peaks of the electronic density at negative curvature close to zero. We can also see among the Zn–P bonds a stronger density, characterized by a repulsion easily seen as a red circle. For the Fm-$3m_2$ structure, bi-colored isosurfaces appear. They result from stabilizing features, counter-balanced by destabilizing interactions due to steric crowding (revealed by the red color). These delocalized interactions form bridge in between the SiP_8 polyhedral. This is probably a signature of the metallic behavior of the compound in this phase.

4 Conclusion

Besides the specific characterization of the bonding properties analyzed here for the $ZnSiP_2$ compound in its inverse phase, there are particular interesting features emerging from the overall analysis of the predicted results in this work. One of the most significant is the response to an applied pressure. As already addressed by an experimental work cited in the text, our theoretical calculation also shows a pressure induced phase transition of the $ZnSiP_2$ compound to a disordered structure. Our new finding is that the entitled compound shows a rearrangement in its bonding

structure at 82GPa for a denser structure with 8 fold, this transition occurs due to the lattice instability found in the disordered structure at 32GPa. However, due to the difficulty to simulate disordered structure within *ab initio* calculations, we could not be able to confirm the stability of the compound at the transition pressure. It would be of great interest to achieve the stability calculations within molecular dynamics, which is, unfortunately, beyond of our capabilities. Our interest in this paper was rather concentrated on bonding evolution that goes along with transition mechanisms. However, we confirm that the $ZnSiP_2$ structure at 32GPa is disordered, and due to the polymerization effect its become ordered at high pressure.

To deep insight of the transition between the ordered parent phases at zero and 82GPa. We propose a transition pathway by following a martensitic (static) approximation, smoothly modeled by a Cc subgroup. The energetic barrier found is less than 100 kJ/mol. The Cc symmetry not only links the I-42d and the Fm-$3m_2$ phases from the symmetric point of view. It also does so from the chemical point of view. From microscopic point of view, using electron localization measure (ELF), we have followed transition mechanism from 4 fold (I-42d) to 8 fold (Fm-$3m_2$). The analysis of the ELF topology has shown that core regions are not affected during the transition mechanism. Moreover, outer-core regions seems to be also slightly affected even if Si-P covalent bonds are weakened in the mechanism. The change in coordination is reflected by a new topological reorganization of charges. The phosphorus basin attractor alters significantly its shape with respect to the other atoms basins forming the Zn–P/Si–P bonds being the key during the transformation path promoting the formation of denser ZnP_8/SiP_8 units at high pressure.

Acknowledgements We would like to thank MALTA Consolider Team and Departamento de Química Física y Analítica, Universidad de Oviedo (Spain), especially, Professor J.M. Recio for giving us access to the computational facilities.

References

1. Gonzalez J, Rincon C (1989) J Appl Phys 65:2031
2. Loferski J. J (1956) J Appl Phys 27:777
3. Frenkel D, Smit B (1996) Understanding Molecular Simulation: From Algorithms to Applications, Academic Press, San Diego
4. Grünwald M, Rabani E, Dellago C (2006) Phys Rev Lett 96:255701
5. Miao M S, Lambrecht W R L (2005) Phys Rev Lett 94:225501
6. Gehlhoff W, Azamat D, Voevodin V G, Hoffmann A (2005) Phys Stat Solidi B 242:R14
7. Magesh M, Arunkumar A, Vijayakumar P, Anandha Babu G, Ramasamy P (2014) Opt Laser Technol 56:177
8. Arab F, Sahraoui F A, Haddadi K, Louail L (2012) Comput Mater Sci 65:520
9. Bhadram V S, Krishna L, Toberer E S, Hrubiak R, Greenberg E, Prakapenka V B, Strobel T A (2017) Appl Phys Lett 110:182106
10. Ouahrani T (2013) Eur Phys J B 86:369
11. Barder R F W (1990) Atoms in molecules. A quantum theory. Clarendon Press, Oxford
12. Contreras-García J, Mori-Sánchez P, Silvi B, Recio J M (2009) J Chem Theory Comput 5:2108
13. Ouahrani T, Franco R, Menendez J M, Marqués M, Recio J M (2014) J Alloy Compd 592:150
14. Martín Pendás A, Costales A, Blanco M A, Recio J M, Luaña V (2000) Phys Rev B 62:13970
15. Becke A D, Edgecombe K E (1990) J Chem Phys 92:5397
16. Silvi B and Savin A (1994) Nature 371:683
17. Kresse G, Joubert D (1999) Phys Rev B 59:1758

18. Perdew J P, Burke K, Ernzerhof M (1996) Phys Rev Lett 77:3865
19. Putz M V (2005) Int J Quantum Chem 105:1
20. Putz M V (2008) Int J Mol Sci 9:1050
21. Savin A, Jepsen O, Flad J, Andersen L K, Preuss H, von Schnering H G (1992) Angew Chem Int Ed Engl 31:187
22. Pilmé J, Renault E, Tahra A, Montavon G, Galland N (2012) J Chem Theory Comput 8:2985
23. Kohout M. (2011) DGrid version 4.6, Radebeul
24. http://elk.sourceforge.net.
25. Johnson E, Keinan S, Mori-Sanchez P, Contreras-Garcia J, Cohen A, Yang W (2010) J Am Chem Soc 132:6498
26. Aroyo M I, Perez-Mato J M, Orobengoa D, Tasci E, de la Flor G, Kirov Bulg A (2011) Chem Commun 43:183
27. Abrahams S C, Bernstein J L (1970) J Chem Phys 52:5607
28. Born M, Huang K (1982) Dynamical Theory and Experiment vol 1 (Berlin: Springer)
29. Capillas C, Perez-Mato J M, Aroyo M I (2007) J Phys : Condens Matter 19:275203
30. Contreras-García J, Recio J M (2011) J Phys Chem C 115:257
31. Salvadó M A, Pertierra P, Morales-García A, Menéndez M, Recio J M (2013) J Phys Chem C 117:8950
32. Krodikis X, Noury S, Silvi B (1997) J Phys Chem A 101:7277